Research Square

Preprints are preliminary reports that have not undergone peer review.
They should not be considered conclusive, used to inform clinical practice,
or referenced by the media as validated information.

Fluorescent lamp tungsten filament thermionic emission gun as a novel humidity optical sensor

Leila Sherafat
Shiraz University
Hossein Torabi-Monfared
Shiraz University
Mohammad Mahdi Doroodmand (doroodmand@shirazu.ac.ir)
Shiraz University
Fazlolah Eshghi
Shiraz University

Research Article

Keywords: Fluorescent lamp, Tungsten filament, Electron gun, Humidity, Optical sensor, Thermionic emission, Image processing.

Posted Date: April 23rd, 2021

DOI: https://doi.org/10.21203/rs.3.rs-434123/v1

License: This work is licensed under a Creative Commons Attribution 4.0 International License.
Read Full License

Abstract

Detecting humidity is a continuing concern within important area such as structural health, food processing, industrial as well agricultural products. In this study, a novel humidity optical sensor is introduced based on the thermionic emission of tungsten filament of a fluorescent lamp. Estimated blue compliant using a charged coupling device camera (CCD) in optical image of the tungsten filament is considered as appropriate detection system for relative humidity (RH) sensing. . The fabricated optical sensor has acceptable linear range (2.0- 98 % RH), improved detection limit (<5.0 % RH), acceptable saturated limit (> 99.0 % RH), improved percentage of relative standard deviation (4.18%, n=2), adequate hysteresis (<4.0 % RH) and a shorter rise time (<5.0 s), respectively. The mechanism behind this detection system was based on the interaction between H2O and tungsten filament during formation of WO3.x H2O (x = 1-2) based on the patented X-ray diffraction analysis.

1. Introduction

For many years, how to measure and monitor the relative humidity (RH) amount has been a matter of debate in different industries, agriculture, and social health [1–3]. For examples, nano-based gas sensors provide significant approach to assess the concentration and environmental information of gases [4,5]. In fact, these sensors comprise of a transducer and an active layer to convert the chemical information into another form of electrical signal gradients like frequency, current, voltage, etc. [6–8]. Their performance characteristic is often based on some different figures of merit including sensitivity, selectivity, detection limit, response time, recovery time, and so on95-8ref). That's why, many research groups have approached to the promotion of humidity-sensitive materials and the current existing manufacturing process [9,10], especially, SnO_2 [11], SiO_2 [12], carbon allotropes [13], zeolites [14] and nano-structure [15].

Nevertheless, regardless of noticeable advantages of these sensors, they are influenced by trials such as small permeability (regarding water molecules), irreversible adsorption/absorption (towards water, that is resulted in dealing with significant memory effects, besides the inadequate hysteresis), and low selectivity (versus H_2O, compared to other organic/inorganic foreign species, especially volatile organic compounds, small sensitive) [16,17]. Albeit, doping different nanostructures to the existing sensors have partially promoted the active surface area, and accessed acceptable permeability and selectivity [18,19]. This process often achieved via following main electrical [20,21] and/or optical [22–24] properties in the manufacturing processes of different RH sensors. Indeed, optical sensors are more useful than the electrical sensing devices, due to the intrinsic features like protection to electrical noises and facility of the miniaturization [22–24]. The main aim of current study is fabricating a novel humidity optical sensor via chemical reaction between water vapor and tungsten based on the thermionic emission of tungsten (W) filament, simply using as fluorescent lamp instrumentation system (gun) with significant advantages such as low cost, availability and/or often simple detection systems.

2. Experimental

2.1. Reagents and materials

Tungsten filament with 2.50 ± 0.03 diameter and electrical resistivity of 2.0 ± 0.1 Ω cm^{-1} was related to the Fras Tungsten Company (Shiraz, Iran). Triply distilled water (Conductivity: 0.5 μS cm^{-1}) was adopted from the combined cycle power plan (Shiraz, Iran) to make the RH standard solutions. Analytical grades of gases with different purities (weight percentages, W/W) such as nitrogen (N_2 99.1%), hydrogen (H_2, 99.996%), carbon monoxide (CO, 99.992%,), carbon dioxide (CO_2, 99 %), argon (Ar, 99.992%) and helium (He, 99.9997%) were from Parsballoon Company (Shiraz, Iran). Also, different volatile organic compounds (VOCs) with analytical grades such as absolute ethanol (Merck Company, 99 %, W/W), diethyl methyl ether (Merck Company, 95 %, W/W), acetone (Flucka Company, 99.0 %, W/W), etc. were selected. In addition, 5.0 ± 0.1 mL of mixture of exhausting gas of a vehicle (L_{90} automobile, Pars Khodro, Class: 56080 2017, Tehran, Iran) was directly sampled inside a tygon tube (200.0 mL, Saint Gobain Fluid Transfer Tygon® F-4040-A, Kyalami Business Park, Kyalami, Midrand, South Africa) to estimate the probable interfering effect(s)

2.2. Instruments

For sensitive and selective RH sensing process, it was focused on the thermionic radiation of tungsten filament as optical detection system. For this purpose, briefly, a new system was designed during formation of the RH standard solutions, ranged between 2.0-98.0 % (±0.1), using a cooling mist piezoelectric-based humidifier (Dyson Pure Humidify + Cool ™ PH01, 12.0 V, Direct Current, DC, China). The humidity system was situated inside a closed cylindrical plastic container (50.0 mL), half filled with the triply distilled water. Introduction of the humidity was achieved via bubbling Ar as carrier gas to the water fluid (from the inlet port of the container), at a fixed flow rate, set by a mass flow controller (MFC), (GE50A013503RMV020 Mass Flow Controller, Germany). The gaseous ample was then transferred towards the analyzing volume from the outlet port of the container. At this condition, the humidity standard solutions (inside Ar gas a solvent) were directly standardized via controlling the Ar flow rate as well as the time duration of the operation of the humidity system and simultaneous monitoring the RH% using a reference RH probe (GCH-2018, ISO-9001, CE, EU).

Image processing of the system was selected as detection system using a charge coupled device (CCD) camera (UOP0600CS, USB 3.0 CCD Camera, Microscope Biological C Mount Microscope Camera, 6.0 Million Pixel, China).

The pressure of the system was also controlled a vacuum pump (Vacuum pump, VP280, 283.0 L min^{-1}, 10.0 CFM, dual stage, Germany). In addition, the temperature of the RH standard solutions was also controlled using a tungsten carbide tubing furnace (length: 20.0 cm, e.d.: 15.0, i.d. 8.0 cm, Azar Furnace Company, Tehran, Iran), situated around the water container.

All the effective parameters such as type of the filament, conditioning the tungsten filament, length of the tungsten filament, electrical applied potential, pressure and the temperature of the system were

automatically controlled using an electronic interface (PCF8591 - 8-Bit Analog Digital Analog Converter ADC/DAC, read relay, 5.0 V DC, analog device, China) through the RS-232 port of a PC and a program software, written in Visual Basic 6 (VB_6).

The probable mechanism of the RH detection system was evaluated using spectroscopic techniques such as middle Fourier transform- infrared (FT-IR, Shimadzu, 8000 Seri, Japan), and patterned X-ray diffraction (XRD, AXS Bruker, US). In addition, a digital caliper (RS PRO, China) was adopted to estimate the length and diameter of the utilized modules in this system.

2.3. Apparatus

Figure 1 shows the schematic of the designed apparatus for the RH detection and measurement. To evaluate the capability of the tungsten filament during interaction with the water molecules, a general fluorescent lamp (Voltage: 220-240 V, AC and power: 20.0 W, KHazar Power, Tehran, Iran) was purchased. After that, the tungsten holder (i.e., electron gun) was separated via cutting the fluorescent tubing from 2.00 ± 0.01 cm higher than the position of the tungsten holder. The gas containing water vapor (humidity) was then introduced to the tungsten filament through a Pyrex glass tubing with 5.0 cm diameter and 1.0 cm height. Argon as carrier gas was also selected as carrier gas through as two-way valves (Brass/Bronze, 12.0 V DC, Normally closed, Two-Way Solenoid Valve, India).

All the system was positioned inside a cylindrical mirror light pipe (MLP, 1415-RP, China) with 5.00 cm diameter and 22.00 cm height. The CCD camera was also introduced to the MLP. The applied AC (alternative current) electrical potential to the tungsten filament was also controlled using as voltage divider analog device through an analog Variac (Variable transformer, 210-240 V, AC, single phase with digital display, Pars Technique, China).

The electrical potential was applied through a three-electrode system, including two florescent electrodes (electrodes: #1 and #2), as the negative-phase pins, which were connected to the two sides (ends) of the tungsten filament inside the analyzing volume. The third electrode included a graphite rod (Electrode #3, Purity: >99.0 %, W/W, length: 2.00 ± 0.01 cm, diameter

2.00 ± 0.01 mm, Saba-Battery company, Tehran, Iran) as the pseudo reference electrode (Null pin). This electrode was connected to the ground (GND) of the electrical supply. At this condition, the electrical current flow from μA to mA levels was correlated to the electron emission process between the tungsten filament and the reference electrode during appearance of the thermionic radiations.

In addition, the electrical current of the thermionic process was amplified through a general fluorescent lamp driver circuit (*220V AC* ,555 Timer IC, 20.0 W, Analog Device, US). The pressure of the cell was also controlled at 25-30 torr using the vacuum pump. This was controlled using as three-way valve Brass/Bronze, 12.0 V DC, Normally closed, Three Way Solenoid Valve, India), positioned inside the MLP. The vacuum of the system was then monitored using a reference vacuum meter (Sunshine Instruments Coimbatore, Tamil Nadu). All the components including, valve, vacuum pump, vacuum meter as well as

the applied voltage to the filament were controlled automatically through an electronic circuit and a computer program written in the VB_6.

2.4. Procedure

Before starting the analysis process, the Ar gas was purged to the analyzing volume with flow rate of 5.0 mL min^{-1} for 2.0 min to have full confidence about the lack of attendance of any oxygen molecule as the oxidant or memory effect(s) of H_2O vapors as analyte in the analyzing volume. After turning off the Ar purging, the pressure of the detection system was set to 25-30 torr using the vacuum pump, along with directly monitoring the pressure by the reference pressure sensor. Then, the AC electrical potential as 1arge as 110 ± 1 V (AC, vs. GND) was applied to the electrode system, and aged for 2.0 min to have complete assurance about the thermal stability as well as steady state condition for the electron emission process. Formerly, the humidifier (humidity system) as well as the MFC were turning on to introduce a fixed RH % standard solution to the analyzing volume, together with simultaneous standardizing using the reference RH probe. This process therefore led to the transient mass terrier of the humidity from the humidity container towards the vacuum system. Afterward, the CCD was set and the photographic images were monitored vs. time. After the analysis process, the electrical power supply, the humidity and the electrical valves were sequentially switched off. The memory effect was subsequently eliminated via following the vacuum processor for 3.0 min for making the system ready for the next analysis process. Summation of blue component of each pixel was selected as the detection system that was estimated using the VB_6 program.

2.5. Real sample analysis

The reliability of this sensor was evaluated via analyses of different real samples such as urban tunnel, lab air, automobile exhaust air, etc. For this purpose, each sample was accumulated in a plastic balloon (30.0 mL) using a membrane pump (Tornado AC580, 12 V DC, 150 psi, China). After cleaning the glass cell as well as elimination of any probable memory effect(s) from the previous analysis, using the procedure reported in the previous section, each sample was introduced to the cell directly with a flow rate of 2.00 ± 0.08 mL min^{-1} for 1.0 min time interval and the images were processed according to the recommended procedure.

2.6. Optimization

In this study, one-at-a time method was selected for the optimization process during image processing. This process was based on estimation of the summation of each red, green and blue (RGB) components (as well as their linear combinations such as R+G, R+B and G+B) of each pixel as the detection system. The reproducibility as well as the reparability of this system were estimated based on the calculation of the percentage of the relative standard deviation (RSD %) during at least three replicate analyses. In addition, the uncertainty of each datum was based on the estimation of the ±RSD (n>3).

3. Results And Discussion

Based on literature, thermionic emission of tungsten filament is considered as one of the most important topics during formation of electron source for bombardment purposes [25]. This system also plays role as a simple and controllable thermal sources for different kinds of thermo-reactions, especially those deal with the endothermic processes [25]. One of the reactions is the chemical interaction between tungsten and water molecules [26,27]. This interaction is often accompanied with formation of thermionic emission (radiation) [25]. The selectivity of this radiation is therefore related to that of the reaction. About some physical processes such as thermal sources that are operated based on the electrical current flow from the filament, formation of radiation is not so selective [25]; whereas when these processes are originated from an electrochemical phenomenon, at constant physical conditions, the selectivity of this process seems to be more acceptable [27]. Based on these phenomena, hereby in this report, for the first time, the electrochemical interaction between the tungsten filament and water molecules is evaluated based on the driving force of the electron radiation. This interaction has therefore resulted in introducing a reliable optical RH sensor

3.1. Structure characterization

Effective interaction between tungsten filament and water molecules were evaluated via spectroscopic methods such as FT-IR spectrometry. It should be noted that, for the preparation of the FT-IR samples, the tungsten element was introduced to a dry KBr powder (Analytical grade, Merck Company) for mechanically contacting with the solid powder. After that, the powder was pressed and analyzed by the FT-IR spectrometer. Based on the FT-IR spectra (Figure 2), the peaks positioned at 3440 and 1604 cm^{-1} were attributed to the formation of adsorbed water [28]. In addition, the peak situated at frequency of 445 cm^{-1} was related to the formation of O-W-O bond [29], as the product during reaction between tungsten filament and water vapor. In addition, major difference was observed between the water interacted W-based filament before (A) and after (B) applying the electrical potential to the system at the optimum conditions. Consequently, significant interaction was evidenced between tungsten and water vapor during the humidity detection and measurement process.

Formation of this reagent was evidenced via surface analyses of the tungsten filament before and after reaction with the water molecules using the driving force of the thermionic electrical current by the XRD spectrometry. The XRD patterns were shown in Figure 3. According to the XRD pattern (Figure 3.A), the peaks positioned at 2θ= 28 and 55 ^{o} were related to the W filament. No changes were observed between the fresh W-filament and that interacted with H_2O vapor (RH: 40-45 %), in the absence of any thermionic electrical current flow. Whereas, after applying the electrical potential (i.e., 110 ± 1 V, AC ,vs. GND) and visualization of the thermionic radiation, appearance of partially sharp peaks (Figure 3.B) at 2θ= 26, 28, 51 and 60 ^{o}, clearly, pointed to the formation of almost WO_3 with (020), (200) (4112) and (311) lattices as the product of the reaction, which agreed with those reported in the literature [30]. In addition, no significant

change was observed between the fresh tungsten filament (A) and that interacted with water, in which the memory effect was eliminated by the recommenced procedure (Figure 3.C).

3.2. Optimization of effective parameters

Parameters having strong influence for the humidity measurement purposes included red, green and blue components, length (resistance) of the filament, applied electrical potential, pressure and the flow rate of Ar as carrier gas. The optimization process was discussed in detail in the following sections.

3.2.1. Selection of RGB components

To reach the highest sensitivity (light intensity) during reaction between tungsten and water molecules, one of the most important parameters was the selection RGB components for having maximum sensitivity and light intensity. As explained before, summation of each R, G and B components of each photographic image was estimated independently, pixel-by-pixel, using the VB_6 program. To optimize this factor, electrical potential ranged the same as 110 ± 1 V (AC, vs. GND) was applied to the tungsten filament with 6.00 ± 0.01 mm length (measured using a micrometer) at 25-30 torr pressure during introduction of standard solution of 40-45% RH. The photographic image during applying 110 ± 1 V (AC, vs. GND) electrical potential has been shown in Figure 4.A. The summations of red, green and blue components of the thermionic radiation during introduction of 40-45 % RH and at the other previously mentioned conditions have been shown according to the histogram shown in Figure 4.B.

Based on the results, maximum sensitivity was observed for the blue component. Therefore, this component was selected as optical probe (analytical signal) during humidity measuring process.

3.2.2. Electrical potential

To optimize the electrical potential, different electrical potentials, ranged between 10 to 220 (± 1) V (AC, vs. GND) were applied to the tungsten filament with 6.00 ± 0.01 mm length and at 25-30 torr pressure. The correlation between the blue component and the electrical potential has been shown in Figure 5.

As shown, due to the flickering effect as well as small lifetime of the tungsten filament during applying high AC voltage, the middle region of the stable region between 100 to 115 (± 1) V (AC, i.e., 110 ± 1 V, vs. GND) was selected as optimum applied voltage.

3.2.3. Effect of pressure

Another factor having important influence on the thermionic radiation was the pressure. To optimum this factor, the system was set during individually setting the pressure of the cell between 5 to 90 torr throughout applying 110 ± 1 V (AC, vs. GND) potential. The results have been shown in Figure 6.

According to the results, maximum sensitivity was observed during applying vacuum condition between 25-30 torr. Therefore, this range was selected as the optimum pressure.

3.2.4. Effect of different lengths of tungsten filament

At constant electrical potential, the length of the tungsten filament directly affected the electrical resistivity and the electrical current flew through the tungsten filament. To optimize this factor, different lengths of the tungsten filament, ranged between 2.00 to 8.00 (±0.01) mm were tested during introduction of 40-45 % RH at the optimum condition. The results have been shown in Figure 7.

Based on the results, a tungsten filament with a thickness of 6.00 ± 0.01 mm was selected as optimum length.

3.2.5. Flow rate of Ar as carrier gas

To optimize the flow rate of the carrier gas, different flow rates of Ar gas were tested through the introduction of 40-45 % RH at the optimum condition such as length of filament 6.00 ± 0.01 mm, RH: 40-45 %, applied voltage: 110 ± 1 V (AC, vs. GND) at 25 $^{\circ}$C. Based on the results, the little fluctuation was observed in the vacuum condition at flow rates larger than 5.00 ± 0.03 mL min^{-1}. Therefore, this flow rate was selected.

3.2.6. Effect of DC and AC electrical potentials

Effect of type of electrical potential on analytical signal (blue component of RGB) was also investigated (Figure 8).

This result indicated that, maximum blue component was provided when AC voltage was applied, versus the DC potential (under similar conditions) at the optimum conditions. This process was almost attributed to the i) segmented thermionic radiations during the applying the AC potential and ii) periodic resting the tungsten figment during the AC alternates.

3.2.7. Effect of temperature

Linear stability was also observed for the fabricated sensor during providing reverse changes between RH % and temperature ranging between 20 to70 ^{o}C for RH 40-45 % (Figure 9).

According to the results, thermal stability of the fabricated sensor at different temperatures was analyzed for a humidity sensing purposes. As maximum sensitivity was observed at temperature between 30 to 35 $^{\circ}$C, therefore this thermal range was selected as optimum temperature of the water vapored prior introduction to the analyzing system.

3.3. Calibration of relative humidity and stability study

The calibration curve of the tungsten-based optical sensor ranging from 2 to 98 % RH has been shown in Figure 10.

The rate of the change in the humidity of the chamber was controlled for having enough time to stabilize the response of the sensor during sweeping the humidity. Based on 90 % of maximum response time (i.e., t_{90}), the response time of the fabricated RH sensor was estimated to be maximum 4.5 s. In addition, the recovery time of the sensor based on 90 % of minimum response (t_{90}) was found to be maximum 5.0 s. The hysteresis during rapid and alternative contacting the optical RH sensor to two sequential conditions such as 20 and 80 % RH during three sequential analyses has been shown in Figure 11.

Satisfied results were observed that revealed the stability as well as the reproducibility of the fabricated RH sensor at the hard conditions. The results were also compared to that of referenced. RH sensor. Minimum difference (<4.0 %, n = 3) was observed between these two RH sensors that revealed the acceptable and stable behavior of the introduced RH sensor during sensing RH % at different real environments.

In this study, detection limit was defined as three folds of the standard deviation of blank to the calibration sensitivity. This value was estimated to less than 0.5 % RH. Due to the hard instrumental conditions of this system, it was not possible to estimate the accurate value for the detection limit. More improved detection limit was evaluated for the tungsten-based humidity optical sensor, in comparison with other types of optical sensors [31–33].

3.4. Selectivity and interference studies

The probable interfering effect of different foreign gaseous species was investigated in the room temperature. For this purpose, the humidity sensor was placed in the chamber and enough excess (at least 100-fold excess) of foreign gases such as CO, CO_2, C_2H_2, CH_4, Ar, He, and volatile organic compounds (VOCs) like ethanol and acetone as well as vapor of acids for instance HCl vapors, individually introduced to the cell at RH = 40-45%. The results are shown in Figure 12.

As shown, no noticeable change in blue parameter clearly revealed the reliability of the fabricated sensor for the trustworthy humidity sensing purpose. This result was not comparable with the thermionic electrical current. In addition, selectivity of proposed sensor was investigated against foreign gases and VOCs. Results exhibited a good selectivity for developed sensor (Figure 13).

3.5. Reusability of the sensor

The reproducibility of fabricated humidity sensor is also shown in Figure 14 at 45-50 % RH. The results revealed acceptable relative standard deviation (RSD %, repeatability as large as 4.18 % (n = 5) for fabricated optical sensor. More reproducibility of the optical imaging process, relative to the thermionic electrical current (7.46 %, n=5), under similar conditions, again pointed to the importance of the image processing for the RH detection purpose.

Also, the RSD % (reproducibility) during analyses of five RH standard samples during at least five replicated analyses was estimated to be 6.05 % (n = 3), again pointed to the acceptable reproducibility of

the sensor for RH sensing purposes. However, pressure dependency of the desorption of this thin layer from the surface of the W filament causes to have reusable (renewability) of the RH optical sensor without any memory effect(s), which was considered as the noticeable feature of this introduced sensing device.

3.6. Real sample analysis

The reliability of the introduced was evaluated via determination of the RH % in different kinds of real gaseous sample, along with comparison with the results analyzed by the reference RH probe, under similar conditions. The results pointed to have relative error percentages as maximum as ±2.31 %, which pointed to the applicability of this RH sensor for the analysis of different real samples.

3.7. Comparison

Comparison between the developed sensor and other sensors, reported in the literature for the RH sensing has been summarized in Table 1. As clearly exhibited, significant figures of merit were estimated for the introduced RH optical sensor, versus different types of RH sensing probes. This comparison therefore approved that, the fabricated RH sensor was considered as satisfactory humidity probe with high accuracy and precision.

Table 1. Comparison between the developed sensor and other RH sensing probes, reported in the literature

Sensor	LDR (% RH)	Response time (s)	Ref.
Depositing the hydrogels poly-hydroxyethyl methacrylate, poly-acrylamide, poly-N-vinyl pyrrolidinone and agarose on optical fiber in order to study their behavior with humidity.	10-100	90.00	31
Highly porous nanostructured titanium dioxide thin film as an optical interference filter	13-71	0.27	34
Spin coated films of Co-Polyaniline nanocomposite for their transmission properties using He–Ne laser	20-95	8.00	35
A hetero-core optical fiber structure that was coated with hygroscopic polymer layers by a layer-by-layer technique, producing a [poly-glutamic acid/poly-lysine] nanostructured overlay	20-90	0.40	32
Microrings assembled with polyacrylamide (PAM) microfibers	5-71	0.12	36
An optical fiber Fabry–Perot interferometric sensors to detect humidity by depositing a hydrophilic coating material on the optical fiber tip	22-80	0.24	33
Thermionic emission of tungsten filament	**2-98**	**≤ 5 s**	**This work**

3.8. Proposed behavior of the fabricated RH sensor

Based on the following evidences, the probable behavior (mechanism) of the RH behavior of the fabricated sensor was attributed to the reaction between the tungsten filament and water vapors. The evidences related to this claim have been summarized as follows:

According to these evidence, the most probable proposed behavior of the fabricated RH sensor were evaluated using spectroscopic techniques such as Fourier transform- infrared spectrometry (FT-IR spectra, Figure 2), X-ray diffraction spectroscopy (XRD patterns, Figure 3). As explained in detail, these analyses pointed to the formation of WO_3 during interaction between the H_2O molecules and tungsten filament.

The chemical reaction between tungsten and water molecules has also been evaluated thermodynamically. Based on the chemical physics studies (53-56), the reactions between the tungsten and the water molecule were endothermic process with apparent activation energy was 132.7 ± 1.1 kJ mol⁻¹ [56] .The thermodynamic reactions are therefore as follows (Eqs. 1-3).

$$W + 2H_2O \rightarrow WO_2 + 2H_2 \quad \text{(Eq. 1)}$$

$$W + 3H_2O \rightarrow WO_3 + 3H_2 \quad \text{(Eq. 2)}$$

$$WO_3 + x\,H_2O \rightarrow WO_3.x\,H_2O \quad (x= 1\text{-}2) \quad \text{(Eq. 3)}$$

As shown, both the thermodynamic and spectroscopic results pointed to the formation of very thin layers of the $WO_3.xH_2O$ as the electrochemical production of the H_2O molecules and tungsten filament at the optimum condition by the driving force of the thermionic current (radiations).

4. Conclusions

Humidity sensor was constructed based on chemical reaction between water vapor and tungsten filament. About this system, optical image of the tungsten filament was considered as an appropriate detection system for the introduced RH sensing device during the image processing using the CCD camera. Parameters having effective influence on the sensitivity of the humidity sensor include conditioning of the tungsten filament, length (resistance) of the tungsten-based filament, electrical potential, effect of vacuum, flow rate of Ar as carrier gas and the temperature. Effect of interferences such as N_2, H_2, CO, CO_2, Ar, He, and different VOCs were considered. The application of this sensor was also evaluated via estimation of RH % in different environmental samples. It can be concluded that (Table 1), the fabricated humidity optical sensor has more improved detection limit (less than 5.0% RH), higher saturated limit (> 99.0% RH), the least relative standard deviation (RSD= 4.18%), shorter rise time (less than 5 s) and also the highest linearity (R^2= 0.9964), compared to those estimated for other types of RH sensors. All the results approve that the fabricated RH sensor is considered as acceptable humidity probe with high accuracy and precision.

Declarations

Acknowledgment

The authors wish to acknowledge the support of this work by the Shiraz University Research Council.

Competing Interests Statement

There are no conflicts to declare.

Author contribution statement

Mohammad Mahdi Doroodmand conceived of the presented idea. Mohammad Mahdi Doroodmand and Hossein Torabi-Monfared developed the theory and performed the computations. Leila Sherafat carried out the analytical method and experiments. Fazlolah Eshghi wrote the manuscript with support from Mohammad Mahdi Doroodmand. All authors discussed the results and contributed to the final manuscript.

References

1. Shivananju, B. N., Hoh, H. Y., Yu, W. & Bao, Q. Chapter 10 - Optical Biochemical Sensors Based on 2D Materials. in *Fundamentals and Sensing Applications of 2D Materials* (eds. Hywel, M., Rout, C. S. & Late, D. J.) 379–406 (Woodhead Publishing, 2019). doi:https://doi.org/10.1016/B978-0-08-102577-2.00010-5.
2. Shinde, P. V, Saxena, M. & Singh, M. K. Chapter 11 - Recent Developments in Graphene-Based Two-Dimensional Heterostructures for Sensing Applications. in *Fundamentals and Sensing Applications of 2D Materials* (eds. Hywel, M., Rout, C. S. & Late, D. J.) 407–436 (Woodhead Publishing, 2019). doi:https://doi.org/10.1016/B978-0-08-102577-2.00011-7.
3. Ascorbe, J., Corres, J., Arregui, F. & Matias, I. Recent Developments in Fiber Optics Humidity Sensors. *Sensors* **17**, 893 (2017).
4. Ge, L. *et al.* Current Applications of Gas Sensor Based on 2-D Nanomaterial: A Mini Review. *Front. Chem.* **7**, 839 (2019).
5. Mirzaei, A. *et al.* Resistive gas sensors based on metal-oxide nanowires. *J. Appl. Phys.* **126**, 241102 (2019).
6. K., A., E., M., G.M., L., J., H. & S., C. A review of gas sensors employed in electronic nose applications. *Sens. Rev.* **24**, 181–198 (2004).
7. Arafat, M. M., Dinan, B., Akbar, S. A. & Haseeb, A. S. M. A. Gas Sensors Based on One Dimensional Nanostructured Metal-Oxides: A Review. *Sensors* **12**, 7207–7258 (2012).
8. Yang, B. *et al.* Aqueous chlorination of benzodiazepines diazepam and oxazepam: Kinetics, transformation products and reaction pathways. *Chem. Eng. J.* **354**, 1100–1109 (2018).
9. Li, Y., Yang, M. J. & She, Y. Humidity sensors using in situ synthesized sodium polystyrenesulfonate/ZnO nanocomposites. *Talanta* **62**, 707–712 (2004).
10. Dabhade, R. V, Bodas, D. S. & Gangal, S. A. Plasma-treated polymer as humidity sensing material—a feasibility study. *Sensors Actuators B Chem.* **98**, 37–40 (2004).
11. Kuang, Q., Lao, C., Wang, Z. L., Xie, Z. & Zheng, L. High-Sensitivity Humidity Sensor Based on a Single SnO2 Nanowire. *J. Am. Chem. Soc.* **129**, 6070–6071 (2007).
12. Zhu, Y., Chen, J., Li, H., Zhu, Y. & Xu, J. Synthesis of mesoporous SnO2–SiO2 composites and their application as quartz crystal microbalance humidity sensor. *Sensors Actuators B Chem.* **193**, 320–325 (2014).
13. Yap, S. H. K., Chan, K. K., Tjin, S. C. & Yong, K.-T. Carbon Allotrope-Based Optical Fibers for Environmental and Biological Sensing: A Review. *Sensors* **20**, 2046 (2020).
14. Kang, S. *et al.* Hydrophobic zeolites coated with microporous organic polymers: adsorption behavior of ammonia under humid conditions. *Chem. Commun.* **51**, 11814–11817 (2015).
15. Buvailo, A. I., Xing, Y., Hines, J., Dollahon, N. & Borguet, E. TiO2/LiCl-Based Nanostructured Thin Film for Humidity Sensor Applications. *ACS Appl. Mater. Interfaces* **3**, 528–533 (2011).

16. Mirzaei, A., Leonardi, S. G. & Neri, G. Detection of hazardous volatile organic compounds (VOCs) by metal oxide nanostructures-based gas sensors: A review. *Ceram. Int.* **42**, 15119–15141 (2016).
17. Spinelle, L., Gerboles, M., Kok, G., Persijn, S. & Sauerwald, T. Review of Portable and Low-Cost Sensors for the Ambient Air Monitoring of Benzene and Other Volatile Organic Compounds. *Sensors* **17**, 1520 (2017).
18. Sharma, A., Kumar, Y., Mazumder, K., Rana, A. K. & Shirage, P. M. Controlled Zn1−xNixO nanostructures for an excellent humidity sensor and a plausible sensing mechanism. *New J. Chem.* **42**, 8445–8457 (2018).
19. Gu, Y. *et al.* Preparation and properties of humidity sensor based on K-doped ZnO nanostructure. *J. Mater. Sci. Mater. Electron.* **30**, 18767–18779 (2019).
20. Ballantine, D. S. & Wohltjen, H. Optical waveguide humidity detector. *Anal. Chem.* **58**, 2883–2885 (1986).
21. Barkauskas, J. Investigation of conductometric humidity sensors. *Talanta* **44**, 1107–1112 (1997).
22. Choi, M. M. F. & Shuang, S. Fluorescent optode membrane based on organogel for humidity sensing. *Analyst* **125**, 301–305 (2000).
23. Kannan, Padmanathan Karthick and Saraswathi, Ramiah and Rayappan, J. B. B. A highly sensitive humidity sensor based on DC reactive magnetron sputtered zinc oxide thin film. *SENSORS AND ACTUATORS A-PHYSICAL* **164**, 8-14. (2010).
24. Zhao, Z. & Duan, Y. A low cost fiber-optic humidity sensor based on silica sol–gel film. *Sensors Actuators B. Chem.* **160**, 1340–1345 (2011).
25. Nottingham, W. B. Thermionic Emission from Tungsten and Thoriated Tungsten Filaments. *Phys. Rev.* **49**, 78–97 (1936).
26. Völkening, J., Köppe, M. & Heumann, K. G. Tungsten isotope ratio determinations by negative thermal ionization mass spectrometry. *Int. J. Mass Spectrom. Ion Process.* **107**, 361–368 (1991).
27. Jousten, K. Pressure measurement with ionization gauges. *CAS - Cern Accel. Sch. Vac. Technol.* **271**, 75–87 (2000).
28. Guéry, C., Choquet, C., Dujeancourt, F., Tarascon, J. M. & Lassègues, J. C. Infrared and X-ray studies of hydrogen intercalation in different tungsten trioxides and tungsten trioxide hydrates. *J. Solid State Electrochem.* **1**, 199–207 (1997).
29. Daniel, M. F., Desbat, B., Lassegues, J. C., Gerand, B. & Figlarz, M. Infrared and Raman study of WO3 tungsten trioxides and WO3, xH2O tungsten trioxide tydrates. *J. Solid State Chem.* **67**, 235–247 (1987).
30. Glemser, O. & Naumann, C. Kristallisierte Wolframblauverbindungen; Wasserstoffanaloga der Wolframbronzen HxWO3. *Zeitschrift fr Anorg. und Allg. Chemie* **265**, 288–302 (1951).
31. Arregui, F. J., Ciaurriz, Z., Oneca, M. & Matíias, I. R. An experimental study about hydrogels for the fabrication of optical fiber humidity sensors. *Sensors Actuators B Chem.* **96**, 165–172 (2003).

32. Akita, S., Sasaki, H., Watanabe, K. & Seki, A. A humidity sensor based on a hetero-core optical fiber. *Sensors and Actuators B-chemical* **147**, 385–391 (2010).
33. Santos, J. S. *et al.* Characterisation of a Nafion film by optical fibre Fabry–Perot interferometry for humidity sensing. *Sensors Actuators B Chem.* **196**, 99–105 (2014).
34. Steele, J. J., van Popta, A. C., Hawkeye, M. M., Sit, J. C. & Brett, M. J. Nanostructured gradient index optical filter for high-speed humidity sensing. *Sensors Actuators B Chem.* **120**, 213–219 (2006).
35. Fuke, M. V, Vijayan, A., Kulkarni, M., Hawaldar, R. & Aiyer, R. C. Evaluation of co-polyaniline nanocomposite thin films as humidity sensor. *Talanta* **76**, 1035—1040 (2008).
36. Wang, P., Gu, F., Zhang, L. & Tong, L. Polymer microfiber rings for high-sensitivity optical humidity sensing. *Appl. Opt.* **50**, G7–G10 (2011).

Figures

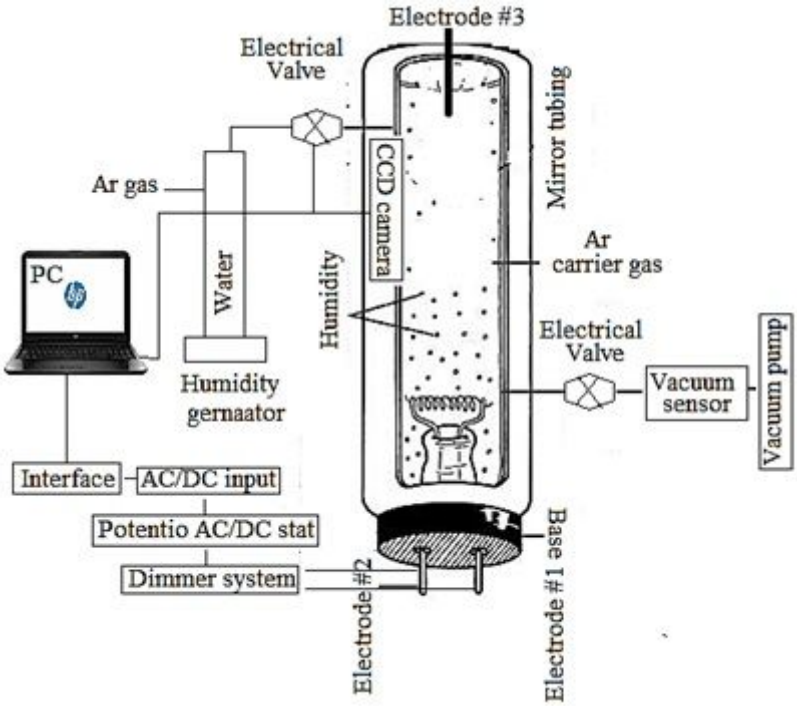

Figure 1

Schematic of the designed apparatus for humidity sensing process.

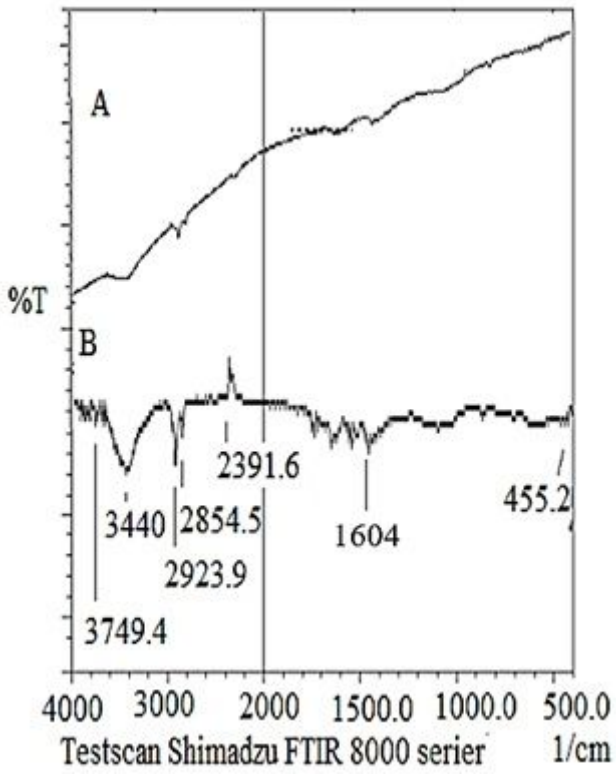

Figure 2

Surface analyses of the tungsten filament by FT-IR spectrometry during interacting with water vapor A) before and B) after applying the electrical potential. Conditions: standard RH: 40-45 %, applied voltages: 110 ± 1 V (AC, vs. GND), and pressure: 25-30 torr.

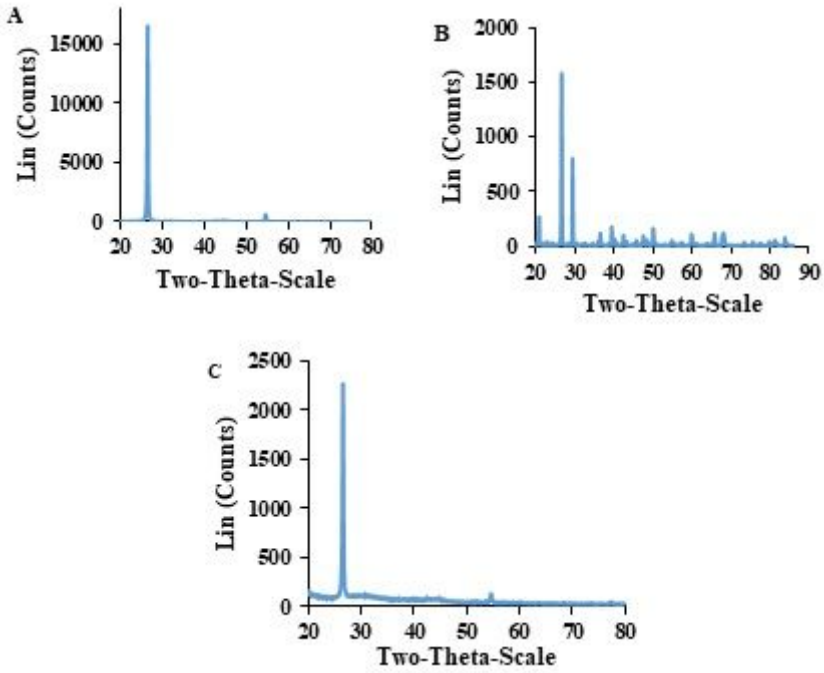

Figure 3

XRD patterns including A) W filament, B) WO3 generated after introduction of humidity and C) W-filament after the elimination of the memory effect. Conditions: standard RH: 40-45 %, applied voltages: 110 ± 1 V (AC, vs. GND), and pressure: 25-30 torr.

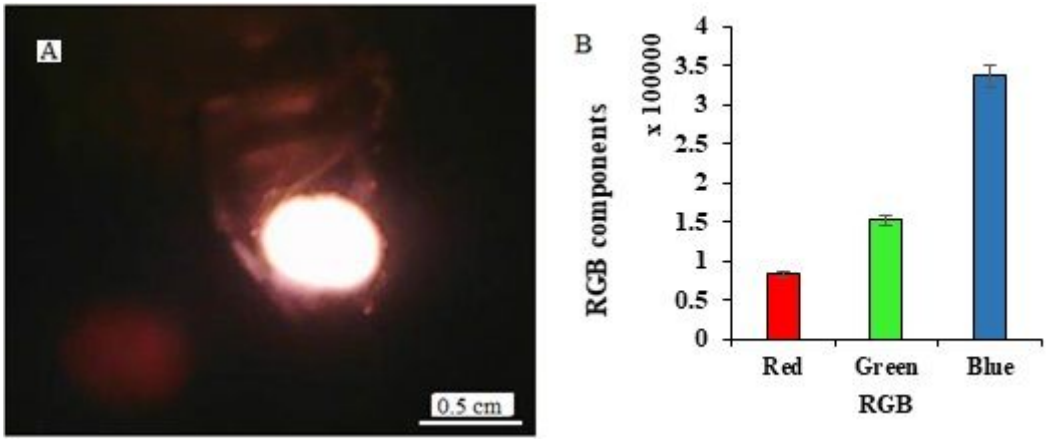

Figure 4

A, B) Photographic image of the thermionic emission of the W-filament and (B) histogram of red, green and blue components during introduction of 40-45% RH during using filament with 6.00 ± 0.01 mm length at 25-30 torr pressure and applying 110 ± 1 V (AC, vs. GND). The data are the average of three independent analyses. Error bar: ± relative standard deviation.

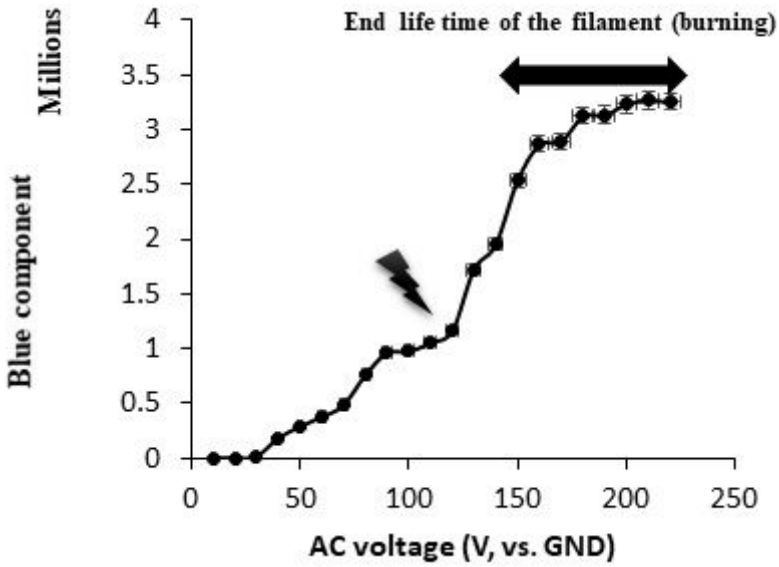

Figure 5

Correlation between the blue components and different applied potential. The data are the average of three independent analyses. Conditions: length of filament 6.00 ± 0.01 mm, RH: 40-45%, and temperature 40-45 °C. The data are the average of three independent analyses. Error bar: ± relative standard deviation.

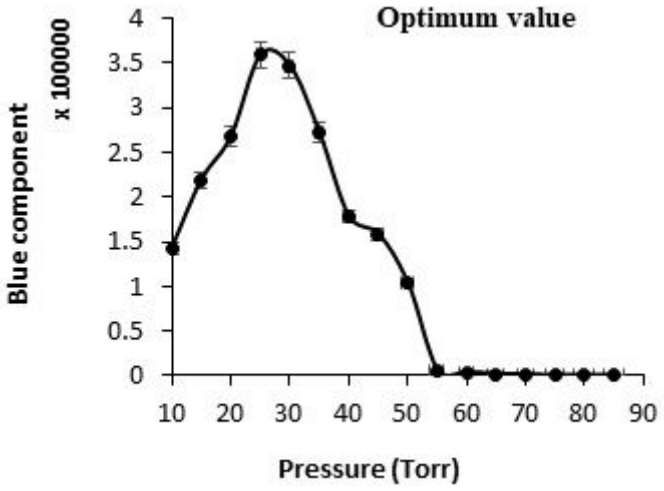

Figure 6

Effect of pressure on the sensitivity of the humidity optical sensor. Conditions: length of filament 6.00 ± 0.01 mm, RH: 40-45%, applied voltage: 110 ± 1 V (AC, vs. GND) and temperature 40-45 °C. The data are the average of three independent analyses. Error bar: ± relative standard deviation.

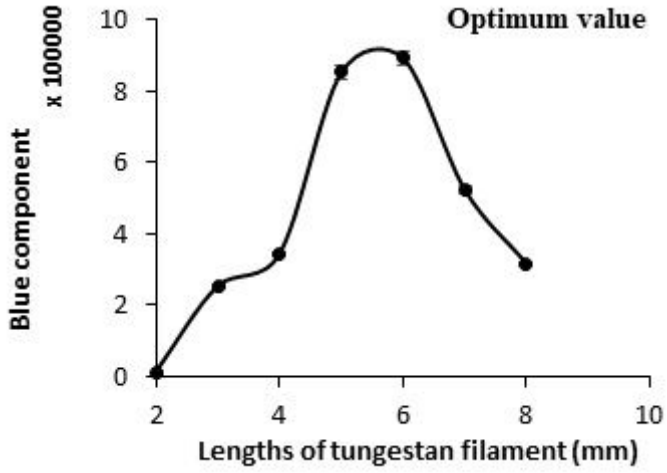

Figure 7

Effect of different lengths of tungsten filament during introduction of 40-45 % RH. Conditions: RH: 40-45%, applied voltage: 110 ± 1 V (AC, vs. GND), pressure: 25-30 torr, and 40-45 °C temperature. The data are the average of three independent analyses. Error bar: ± relative standard deviation.

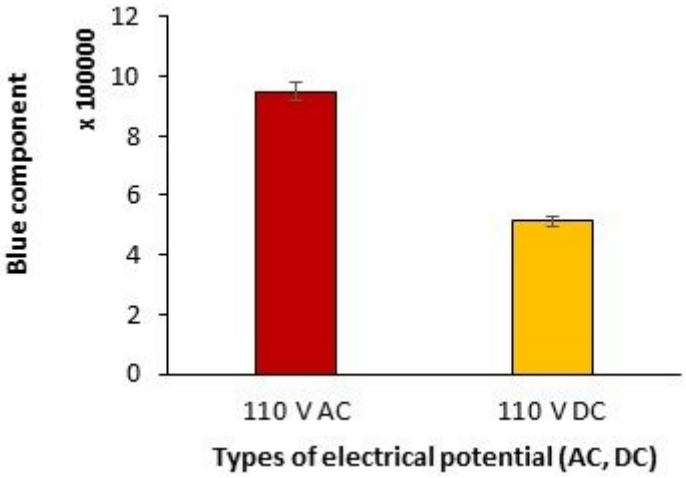

Figure 8

Effect of AC and DC electrical potential on analytical signal. Conditions: RH: 40-45%, applied voltages: 110 ± 1 V (AC, DC, vs. GND), pressure: 25-30 torr, and temperature 40-45 °C. The data are the average of three independent analyses. Error bar: ± relative standard deviation.

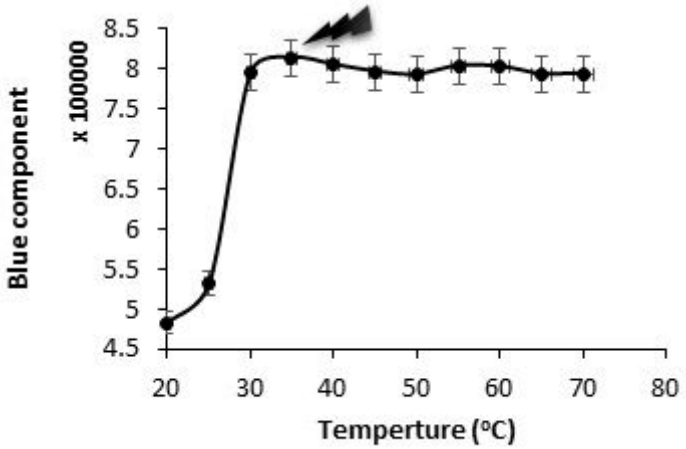

Figure 9

Optimum temperature for water vapors introduced to the analyzing system. Conditions: standard RH: 40-45 %, applied voltages: 110 ± 1 V (AC, vs. GND), and pressure: 25-30 torr. The data are the average of three independent analyses. Error bar: ± relative standard deviation.

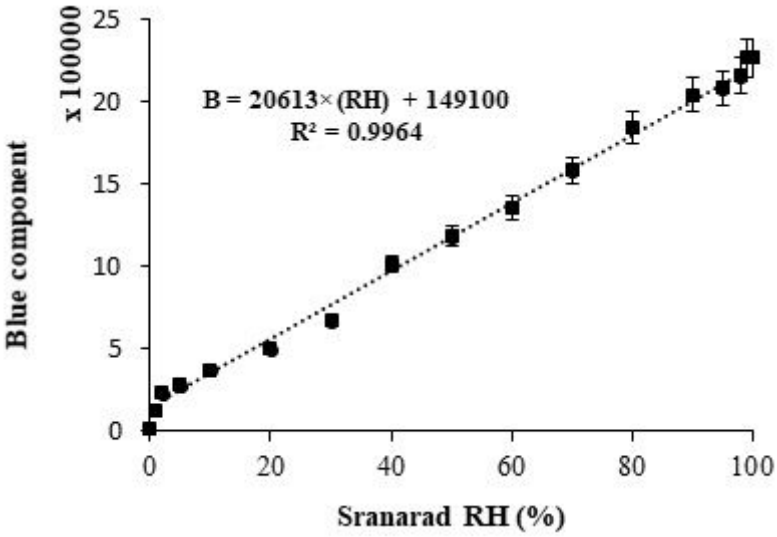

Figure 10

Calibration curve of RGB parameter vs. %RH. Conditions: standard RH: 0-100 %, applied voltages: 110 ± 1 V (AC, vs. GND), pressure: 25-30 torr, and temperature 40-45 °C. The data are the average of three independent analyses at optimum conditions. Error bar: ± relative standard deviation.

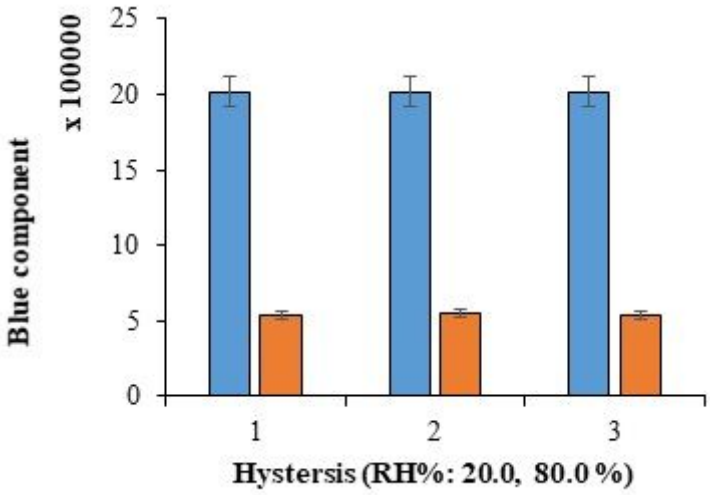

Figure 11

Diagram representing the hysteresis of the fabricated sensor Conditions: standard RH: 20 and 80 % (Sequential introduction), applied voltages: 110 ± 1 V (AC, vs. GND), pressure: 25-30 torr, and temperature 40-45 °C. The data are the average of three independent analyses. Error bar: ± relative standard deviation.

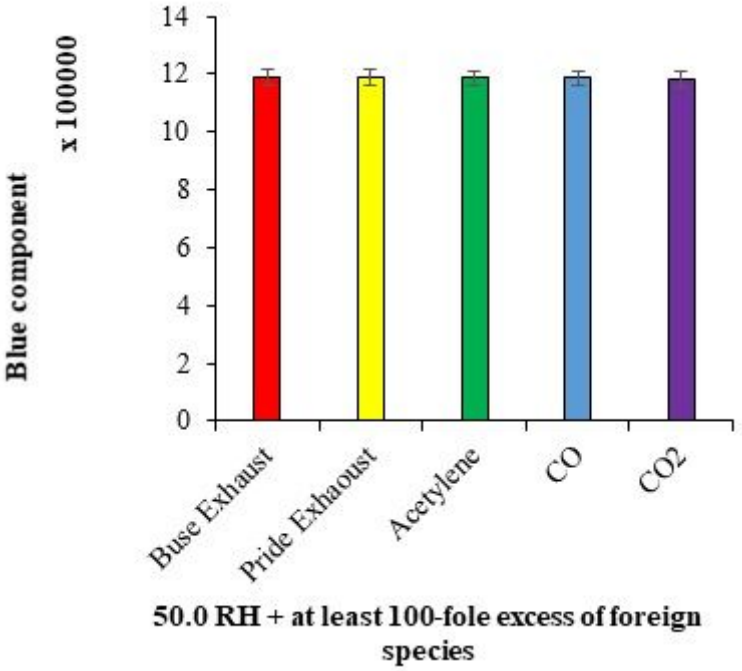

Figure 12

Effect of coexisting species on the performance of –tungsten-based RH sensor during spiking into a standard RH %. Conditions: standard RH: 50.0 %, applied voltages: 110 ± 1 V (AC, vs. GND), and pressure: 25-30 torr. The data are the average of three sequential analyses at optimum conditions. Error bar: ± relative standard deviation.

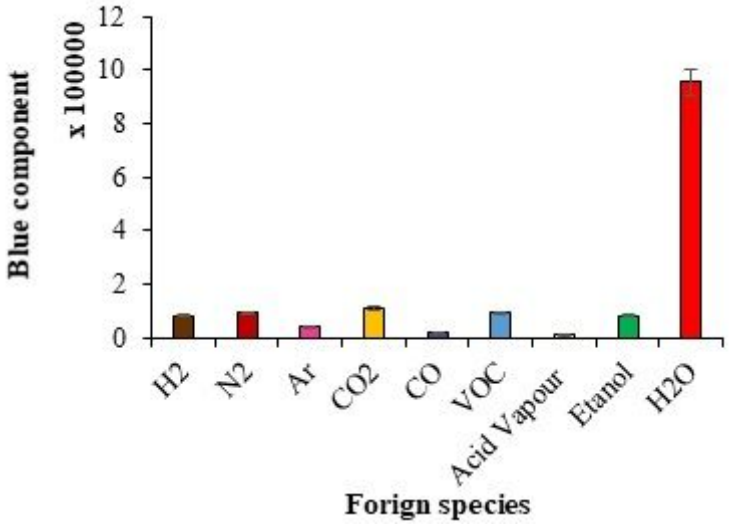

Figure 13

Selectivity of developed sensor. Conditions: standard RH: 40-45 %, applied voltages: 110 ± 1 V (AC, vs. GND), and pressure: 25-30 torr. Tolerance ratio: at least 100-fold excess. The data are the average of three independent analyses at optimum conditions. Error bar: ± relative standard deviation.

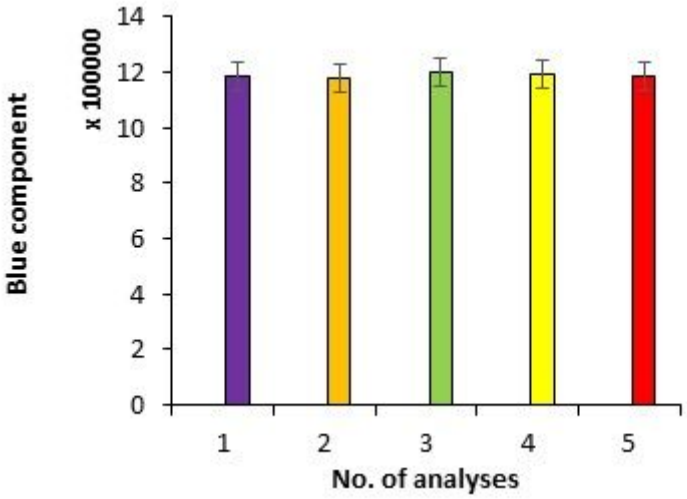

Figure 14

Reproducibility of fabricated RH sensor during contacting RH standard solution. Conditions: standard RH: 40-45 %, applied voltages: 110 ± 1 V (AC, vs. GND), and pressure: 25-30 torr. The data are the average of three independent analyses. Error bar: ± relative standard deviation.